Breaking Symmetry of Single-Atom Catalysts Enables Extremely Low Energy Barrier and High Stability for Large-Current-Density Water Splitting

Xueqin Mu
Wuhan University of Technology
Xiangyao Gu
Nanjing Xiaozhuang University
Shipeng Dai
Nanjing Xiaozhuang University
Jiabing Chen
Nanjing Xiaozhuang University
Qu Chen
Nanjing Xiaozhuang University
Min Yu
Nanjing Xiaozhuang University
Changyun Chen
Nanjing Xiaozhuang University
Wenxing Chen
Beijing Key Laboratory of Construction Tailorable Advanced Functional Materials and Green Applications, School of Materials Science and Engineering, Beijing Institute of Technology
https://orcid.org/0000-0001-9669-4358
Suli Liu
Nanjing Xiaozhuang College
Shichun Mu (msc@whut.edu.cn)
1. State Key Laboratory of Advanced Technology for Materials Synthesis and Processing, Wuhan University of Technology, Wuhan 430070 https://orcid.org/0000-0003-3902-0976

Article

Keywords: heteroatomic interfaces, electrochemical water splitting, large-current–density, layered double hydroxides, single Ru atoms

Posted Date: March 9th, 2022

DOI: https://doi.org/10.21203/rs.3.rs-1409828/v1

Abstract

The instability and low large-current-density efficiency for a single atomic metal species system have aroused widespread concern. Herein, the Ru single-atom system constructed on iron–cobalt layered double hydroxide (Ru_x SACs@FeCo-LDH) exhibits extremely low oxygen evolution reaction (OER) overpotentials of 194 and 246 mV at current densities of 10 and 1000 mA cm^{-2}, respectively, and high stability beyond 1000 h at 1000 mA cm^{-2}, far surpassing commercial RuO_2. Moreover, its mass activity is ~2 and 6 times higher than that of Ru and FeCo-LDH, respectively. Extraordinarily, it only needs 1.52 V to achieve 1000 mA cm^{-2} current densities for water-splitting, and is almost unchanged after 1000 h, as the highest performance reported so far. Experimental and theoretical calculation results evidence that, partial substitution of oxophilic-Ru atoms to FeCo-LDH triggers the reconstruction at symmetry breaking interfaces, promoting O-O coupling at Ru-O active sites for OER, beneficial for suppressing multiple heteroatomic interface instability under large-current-density water-splitting. Our strategy opens up opportunities for lifting single-atom stability in industrial-scale hydrogen production from water-splitting.

Introduction

Hydrogen production through electrochemical water splitting is an efficient strategy for sustainable and green energy source.[1] Conventionally, Pt, Ir or Ru-based serve as the highly efficient electrocatalysts for hydrogen evolution reaction (HER) and oxygen evolution reaction (OER) as two half-reactions in water splitting.[2,3] However, their overpotentials to reach large current densities of 1 A cm^{-2} for practical large-scale water electrolysis is still very high (>300 mV). Furthermore, their scarcity, high cost and relatively low durability limit the commercial prospect.[3-5] Therefore, developing cost-effective and abundance in raw materials or ultralow noble metal usage, with durable electrocatalysts for meeting the requirements of practical water electrolysis, becomes the key for water splitting at high current densities.

Iron–cobalt layered double hydroxide (FeCo-LDH) with unsaturated coordination sites are favorable for applications in simultaneously catalyzing the HER and OER under alkaline conditions.[6,7] However, to satisfy the industrial requirements of large current densities (≥1 A cm^{-2}) at low overpotential (<300 mV), with over long-term durability (over 1000 h), further improvement of the catalysts for OER is inevitable. To optimize the catalytic activity of LDH, one approach is to facilitate the electron transfer by tailoring the interfacial interactions and coordination/electronic environment via a “breaking the symmetry” strategy.[8-10] For example, it is effective to control growth of LDH (e. g. Fe, Co) with alternating Fe and Co atoms arrangements via doping foreign single atoms, leading to a localized excess of charge due to the polarization associated with symmetry-breaking structures.[7,11] More importantly, doping LDH substrates with another atom as new active sites could induce the systematic optimization of charge transfer at their heteroatomic interfaces and boost the oxygen evolution performance.[12-15] Subsequently, the partial substitution effect could suppress the multiple heteroatomic interface instability in industry-scale hydrogen production from water splitting. However, how to break the symmetry structure and construct a

stable multiple atomic heterointerface on LDH become significant but challenging for high-current-density water splitting.

In this work, we propose that oxophilic-metal (Ru) species single-atomic-site doping in FeCo-LDH (Ru SACs@FeCo-LDH) can effectively break the FeCo-LDH symmetry structure, and lead to the active atom reconstruction at symmetry breaking interfaces, which is essential to achieve an excellent catalytic activity for OER. As a result, the Ru_x SACs@FeCo-LDH is designed and built by a simple approach, which delivers a large-current-density of 1000 mA cm^{-2} at an ultralow overpotential of 246 mV and keeps a high stability over 1000 h. In addition, the superior HER performance of Ru_x SACs@FeCo-LDH is similar to the commercial Pt catalyst. Logically the assembled two-electrode cell with Ru_x SACs@FeCo-LDH reaches an industrial current density of 500 and 1000 mA cm^{-2} for overall water splitting in alkaline media at low cell voltages of 1.47 and 1.52 V, respectively. Experimental and DFT calculation results confirm the existence of the Ru single-atomic-site and the unusual symmetry-breaking phenomenon, which forms a region of charge transfer at the heteroatomic interfaces, exhibiting greatly enhanced electrochemical performance towards OER and overall water splitting.

Results And Discussion

Ru SACs@FeCo-LDH was constructed by a mixed-solvent strategy. As illustrated in **Figure 1a**, Ru SACs@FeCo-LDH is fabricated by first growing FeCo-LDH arrays using Ni foam as substrate, followed by in situ growth of single-atomic-site on FeCo-LDH arrays. To optimize catalytic activity, Ru_x SACs@FeCo-LDH with different molar ratios of Ru precursors is named as Ru_1 SACs@FeCo-LDH and Ru_2 SACs@FeCo-LDH (Table S1). In addition, by ICP test, the content of Fe, Co, and Ru for Ru_1 SACs@FeCo-LDH is ~ 0.236, 0.450 and 0.508 wt%, the content of Fe, Co, and Ru for Ru_2 SACs@FeCo-LDH is ~ 0.013, 0.009 and 1.532 wt%, respectively. Transmission electron microscopy (TEM) and field emission scanning electron microscopy (FE-SEM) images reveal that Ru_1 SACs@FeCo-LDH still maintains the uniform 3D porous structure composed of interconnected ultrathin nanosheets with a smooth surface and sharp edges (**Figure 1b**). As shown in Figure S1, Ru_1 SACs@FeCo-LDH also exhibits the shape of nanosheets with small size and multiple twin interfaces formed by heteroatomic doping. The spherical aberration corrected HAADF-STEM images in **Figure 1c** and S2 confirm a 3D porous FeCo-LDH nanosheets structures for Ru_1 SACs@FeCo-LDH. Meanwhile, many bright dots are randomly distributed on the surfaces of FeCo-LDH nanosheets without any apparent nanoclusters. And no typical peaks can be observed in the XRD pattern (Figure S3), possibly indicating the formation of single atom on the FeCo-LDH. Notably, we unlock an unusual symmetry-breaking structure with asymmetric Fe/Co interfaces containing defective segments in Ru_1 SACs@FeCo-LDH (**Figure 1d and 1e)** and Ru_2 SACs@FeCo-LDH **(**Figure S1 and S4). Furthermore, rich porous structures are formed due to the asymmetric coordination of Fe/Co atoms around Ru atom, which is conducive to the increase in specific surface area resulting in the increase in active area in the OER process.[16] The above results confirm that Ru atoms enter the lattice by replacing partial Fe/Co atoms. **Figure 1f** reveals an ultrathin nature of Ru_1

SACs@FeCo-LDH nanosheets, with a thickness of only about 3.09 nm. The energy-dispersive X-ray (EDX) spectroscopy further demonstrates a homogeneous distribution of the Fe, Co, and Ru species (**Figure 1g** and S5). All the above results indicate that Fe, Co, and Ru elements are homogeneously dispersed on the FeCo-LDH substrate.

To clarify the specific localizations of metal atoms on FeCo-LDH substrate, X-ray photoelectron spectroscopy (XPS) (Figure S6) and X-ray absorption fine structure (XAFS) spectroscopy analysis were performed. The element atomic content of the Ru_1 SACs@FeCo-LDH is shown in the Table S2. The Fe $2p_{3/2}$ and Fe $2p_{1/2}$ peaks of Ru_1 SACs@FeCo-LDH are located at 711.06 and 723.50 eV, respectively, which are assigned to Fe(Ш) (Figure S7).[12,17] In the Co $2p_{3/2}$ narrow scan XPS spectrum (Figure S8), the peaks at 797.58 and 796.11 eV correspond to the Co^{2+} and Co^{3+} species, respectively.[18] Meanwhile, compared with FeCo-LDH, the binding energy of the Co species on Ru_1 SACs@FeCo-LDH negatively shifts by approximately 0.65 eV, indicating a higher electron density of Co species than that on FeCo-LDH.[18,19] Besides, the higher binding energy of Ru 3p suggests the presence of oxidized Ru^{x+} species for Ru_x SACs@FeCo-LDH (Figure S9). In addition, as displayed in Figure S10, three peaks can be clearly identified at 532.7, 531.6 and 530.9 eV, which are assigned to M–OH, oxygen atoms bound to oxygen vacancies (O_{vac}) and M-O, respectively. [20] Notably, compared with FeCo-LDH, the binding energy for lattice oxygen of Ru_1 SACs@FeCo-LDH shifts to a lower level (530.2 eV), possibly due to the change of electronic state for lattice oxygen induced by Ru-doping.[20]

Furthermore, the coordination environment and chemical state of Ru_1 SACs@FeCo-LDH were further investigated by both Co, Fe, and Ru K-edge X-ray absorption fine structure (XAFS) spectroscopy. The Fe K-edge XANES spectra of Ru_1 SACs@FeCo-LDH and FeCo-LDH samples show distinct pre-edge peaks at ≈ 7133.2 eV (**Figure 2a**), in which the absorption edge of these samples is close to that of Fe_2O_3, indicating that the atomically dispersed Fe species carries positive charge of ~+3.[21] Meanwhile, the absorption edge of Co K-edge of Ru_1 SACs@FeCo-LDH and FeCo-LDH is located between CoO and Co_3O_4, demonstrating that the valence state of Co species is between +2 and +3 (**Figure 2b**).[22] The Ru K-edge XANES spectra of Ru_1 SACs@FeCo-LDH and Ru_2 SACs@FeCo-LDH in **Figure 2c** show that the edge energy is between Ru foil and RuO_2, demonstrating a cationic environment.[23] The Fourier transforms of EXAFS spectra (FT-EXAFS, without phase correction) in **Figure 2d** reveal a peak at R = 1.5 Å corresponding to Fe–O bonds, and the typical peak appears at 1.6 Å in the EXAFS spectrum for Co K-edge of Ru_1 SACs@FeCo-LDH (**Figure 2e**), due to the presence of Co-O sites of atomic Co coordinated with O on LDH. Notably, the corresponding Fourier transform of the EXAFS profile was fitted by Ru-O paths (**Figure 2f**), reflecting that the Ru element in Ru_1 SACs@FeCo-LDH or Ru_2 SACs@FeCo-LDH is single-atom dispersed. In addition, the wavelet transforms (WT) of EXAFS spectrum for Fe, Co, and Ru K-edge (**Figure 2g-2i**) of Ru_1 SACs@FeCo-LDH shows the characteristic peak of the Fe (Co, Ru)-O bond at 2.4 Å that can be assigned to atomic Fe (Co, Ru)-O species. This further confirms that Ru SACs@FeCo-LDH is virtually the FeCo-LDH-supported and -stabilized single Ru atom catalyst.

To explore the influence of the Ru single-atom modified FeCo-LDH toward OER, we evaluated the OER activity of Ru_x SACs@FeCo-LDH, together with those of FeCo-LDH, Ru and blank Ni foam as benchmark in O_2-saturated 1.0 M KOH solutions. As shown in **Figure 3a** and S11, it can be seen that blank Ni foam requires an overpotential of 439 mV at a current density of 500 mA cm^{-2}, and decreases to 320 mV after the formation of FeCo-LDH on Ni foam. Furthermore, after the incorporation of single-atomic-Ru species, Ru_1 SACs@FeCo-LDH exhibits the best OER performance (**Figure 3a**), realizing the ultralow overpotential of 194 and 230 mV at 10 and 500 mA cm^{-2}, respectively. Meanwhile, Ru_1 SACs@FeCo-LDH presents the smallest Tafel slope of 25 mV dec^{-1}, much lower than that of FeCo-LDH (49 mV dec^{-1}), blank Ni foam (93 mV dec^{-1}), and Ru (34 mV dec^{-1}) (**Figure 3b**), respectively.

Apparently, at elevated current densities, Ru_1SACs@FeCo-LDH still has a favorable oxygen evolution kinetics. **Figure 3c** shows the comparison of overpotentials under current densities of 1 A cm^{-2}. The OER activity of other catalysts increases in the following order: Ru < IrO_2 < FeCo-LDH < RuO_2 < Ru_1 SACs@FeCo-LDH, demonstrating the excellent OER performance for Ru_1 SACs@FeCo-LDH. In detail, it possesses a small overpotential as low as 246 mV at 1A cm^{-2} for Ru_1 SACs@FeCo-LDH, which is 89 and 165 mV lower than that of the state-of-the-art FeCo-LDH and Ru catalysts, respectively (**Figure 3c**). Correspondingly, at such a high current density, it shows a much lower overpotential than that of commercial RuO_2 (280 mV) and IrO_2 (375 mV), further demonstrating the best electrocatalytic OER activity of Ru_1 SACs@FeCo-LDH at either small or large current densities (such as 1A cm^{-2}), even better than most of previously reported catalysts (**Figure 3d** and Table S3).

Moreover, for Ru_1 SACs@FeCo-LDH, its mass activity (MA) at η = 200 mV is ~6 times higher than that of the FeCo-LDH, and still ~2 times higher than that of the Ru catalyst (**Figure 3e**), confirming the enlargement of the active sites due to the introduction of Ru. Even at larger overpotentials, the MA of Ru_1 SACs@FeCo-LDH reaches a surprising value, far exceeding that of the contrast catalyst. Extraordinarily, the TOF at η=200 mV was calculated to be 7.17×10^3 s^{-1}, by assuming that all Co, Fe, and Ru atoms in Ru_1 SACs@FeCo-LDH (**Figure 3f**), which is the highest TOF value in comparison with the reported catalysts (Table S3).[24] We also confirm the fast kinetics of Ru_1 SACs@FeCo-LDH using electrochemical impedance spectroscopy (EIS) (**Figure 3g** and S12). From Nyquist plots, the charge transfer resistance (R_{ct}) of Ru_1 SACs@FeCo-LDH is the smallest among the control samples under the same conditions, demonstrating much faster kinetics for OER after introduction of Ru single atoms.[25]

More importantly, for a practical electrocatalyst, it is important to maintain good stability over long-term use (over 1000 h), however this is very challenging especially at large current densities. As shown in **Figure 3h and 3i**, for Ru_1 SACs@FeCo-LDH, there is no apparent attenuation of the current density of 1 A cm^{-2} over 1000 h and even after 20000 continuous cycles, verifying remarkable long-term stability for Ru_1 SACs@FeCo-LDH. Meanwhile, to further provide the role of surface single atoms on water dissociation kinetics, SEM and XPS analyses were performed. As shown in **Figure 3i** and S13, after the OER process,

the peak area ratio (Co^{3+}/Co^{2+}) increases greatly, which indicates the real catalytic site of LDH-based catalysts would gradually change to oxyhydroxide (Co, Fe-OOH) as a structural reconstruction during the OER process.[14]

Besides the OER, the HER electrocatalytic activity of different samples was probed in alkaline solutions (1.0 M KOH). As depicted in **Figure 4a** and S14, as expected, Ru_2 SACs@FeCo-LDH with increased Ru loading exhibits superior HER activity in alkaline media with a near-zero onset overpotential, with the corresponding Tafel slope as low as 53 mV dec^{-1} (**Figure 4b**), exhibits obvious similar activity to Pt-C and superior to FeCo-LDH and Ru catalysts. As shown in **Figure 4c**, to achieve the current densities of 500 and 1 A cm^{-2}, it only needs overpotentials of 84 and 117 mV for Ru_2 SACs@FeCo-LDH, displaying the best alkaline HER activity, very close to that of the commercial Pt/C (78 mV@500 mA cm^{-2}, 110 mV@1 A cm^{-2}), but much lower than those of FeCo-LDH (204 mV@500 mA cm^{-2}, 250 mV@1 A cm^{-2}) and Ru (324 mV@500 mA cm^{-2}, 363 mV@1 A cm^{-2}). It is worth mentioning that the HER performance of Ru_2 SACs@FeCo-LDH is higher than most of the reported hybrid electrocatalysts (**Figure 4d** and Table S4). Meanwhile, from **Figures 4f** and S15, Ru_2 SACs@FeCo-LDH gives the largest C_{dl} of 328 mF cm^{-2} and the smallest R_{ct} of 0.92 Ω (**Figures 4g** and S16), suggesting the faster HER kinetics due to greatly improved electrochemical surface area and charge transfer capability. Importantly, Ru_2 SACs@FeCo-LDH displays an excellent stability with a negligible degradation during long-term test, with an ignorable loss of overpotential at 1 A cm^{-2} over 1000 h (**Figure 4h**). Besides, no obvious morphology and structural changes can be observed from the characterization of Ru_2 SACs@FeCo-LDH after HER stability test (Figure S17).

Considering the outstanding OER performance of the bifunctional Ru_1 SACs@FeCo-LDH and Ru_2 SACs@FeCo-LDH electrocatalyst, we assembled an alkaline electrolyzer using these catalysts as both the anode and cathode in 1.0 M KOH solutions (**Figure 5a** and S18). Impressively, such an electrolyzer exhibits the best overall water splitting activity among all samples (**Figure 5b**). In detail, to deliver the current densities of 500 mA cm^{-2} and 1 A cm^{-2}, Ru_x SACs@FeCo-LDH merely requires the lowest voltages of 1.47 and 1.52 V, respectively, much lower than those of FeCo-LDH‖FeCo-LDH (1.83 and 1.97 V), Ru‖Ru (1.68 and 1.96 V), and Pt-C‖IrO_2 (1.74 and 1.92 V), respectively. Moreover, from **Figure 5c** and S18, the Faradaic efficiency of the bifunctional Ru_x SACs@FeCo-LDH electrocatalyst cell was estimated to be >99%, indicating that the high selection for water splitting.[26] More importantly, negligible decay in applied potentials for Ru_x SACs@FeCo-LDH can be observed by the continuous test over 1000 h at 1 A cm^{-2}, indicating excellent durability (**Figure 5d**). Compared to the reported electrocatalysis under large current densities (e.g., 500 and 1000 mA cm^{-2}), all aforementioned analysis confirms that as-prepared Ru_x SACs@FeCo-LDH catalysts can be served as promising industrial candidate catalyst for industrial-scale overall water splitting (**Figure 5e** and Table S5).

Discussion

Density functional theory (DFT) calculations were further performed to elucidate the inherent relationship between the synergistic effect of electronic structure and catalytic activity of the oxophilic-metal (Ru) species doped on FeCo-LDH (Ru SACs@FeCo-LDH) under alkaline conditions. After introducing Ru sites, the interface symmetry structure of FeCo-LDH can be broken due to the partial substitution of FeCo sites, which is evidenced by the AC-STEM observation result. Thus, Ru SACs@FeCo-LDH formed generates new electronic states near the Fermi level, suggesting a more conductive electronic structure (**Figure 6a**).[27] This can be further evidenced by the partial density of states (PDOS) caused by the change of electronic structure of Co, Fe, and Ru (**Figure 6b**). It is noteworthy that after Ru doping the DOS projected on Co *d* orbital shifts to lower energies. The shift results in the reduction of the DOS near the Fermi level and the *d*-band center make the adsorption weaker and the desorption of adsorbed intermediates easier, which is necessary for OER. [28] Correspondingly, the reaction pathways of alkaline OER include four steps ($G1$: * → *OH; $G2$: *OH → *O; $G3$: *O → *OOH; $G4$: *OOH → 1/2 O_2) (**Figure 6c and 6d**), accompanied by the formation of a series of intermediates, such as OH*, O*, OOH*, and OO*.[12,20] The optimized pathways of various sites are shown in Figure S19. Based on the free energy diagram (**Figure 6c**) of FeCo-LDH, the energy barrier ($\Delta G4$ = 0.488 eV) for the O_2 desorption is the rate-determining step on the Co site. After introducing Ru into FeCo-LDH, the Ru site (**Figure 6d**) generates and enhances the adsorption energy of the OER intermediates. As a result, the rate-determining step on Ru site for Ru SACs@FeCo-LDH is the formation of *OH with a smaller energy barrier of 0.191 eV. The decrease of energy barrier after incorporating Ru atom into the FeCo-LDH catalyst implies that the unique electronic structure in the three single-atomic-site of Ru SACs@FeCo-LDH plays a vital role in improving OER activity. What is more, the decrease of the energy barrier can better verify the effect of Ru atoms on the original lattice of Co and Fe, which breaks the interface symmetry structure of FeCo-LDH and creates more active sites, making the catalytic reaction easier to occur.[12,29]

In addition, the *d*-band center was calculated by the *d* orbital of the active site, and the change curve of the adsorption free energy with the three intermediates (G_{OH*}, G_{O*}, G_{OOH*}) was obtained (**Figure 6e**). Obviously, the introduction of Ru atoms leads to nearing the Fermi level, facilitating the OER activity (**Figure 6e**). Meanwhile, as shown in **Figure 6f,** the overpotential for OER can reach the "volcano" peak when the *d*-band center is applicable. By comparing the oringinal FeCo-LDH, we can see that Ru doping individually decreases the overpotential (**Figure 6f**). Compared with the Co sites on the interfaces of FeCo-LDH and Ru SACs@FeCo-LDH, the reaction energetics is the significantly optimized (**Figure 6g**). In addition, the trend holds true for Fe and Ru sites as well (Figures S20-S22). Thus, doping Ru atoms indeed lowers the overpotentials of all compounds and expands the active catalytic site. The Co ligand is slightly distorted when Ru atom is doped into FeCo-LDH crystal lattice because of the larger radius of Ru atoms than that of Co atoms. Such symmetry-breaking forms the strongly coupled Schottky interface between Ru single-atoms and FeCo-LDH matrix, leading to the significant changes in electronic structure.[30-32]

Overall, the above theoretical calculations are consistent with the experimental results, which prove that the modulated reaction pathway and free energy of FeCo-LDH by Ru SACs doping can achieve higher OER and HER performance.

Conclusions

In conclusion, to optimize heteroatomic interface and mass transfer toward high-current-density overall water splitting, the strong coupled single-atom (e. g. Ru) modified iron–cobalt layered double hydroxide on Ni foam (Ru_1 SACs@FeCo-LDH) were constructed. The as-obtained Ru_x SACs@FeCo-LDH exhibited excellent electrocatalytic activity and stability toward OER and overall water splitting, especially at large-current-density of 1000 mA cm^{-2}. Experimental analysis and DFT calculation results unlocked that, due to the partial substitution of FeCo-LDH by oxophilic-metal (Ru) atoms, the long-range order of heteroatomic interface can be broken, and then the active atom reconstruction at symmetry breaking interfaces occurred. This led to the strongly coupled Schottky interface between Ru single-atoms and FeCo-LDH matrix and extraordinary high-overall water splitting performance under industrial-grade current densities.

References

1 Nishiyama, H. *et al.* Photocatalytic solar hydrogen production from water on a 100-m^2 scale. *Nature* **598**, 304-307 (2021).

2 Jiao, S., Fu, X., Wang, S. & Zhao, Y. Perfecting electrocatalysts via imperfections: towards the large-scale deployment of water electrolysis technology. *Energy Environ. Sci.* **14**, 1722-1770 (2021).

3 Zhuang, Z. *et al.* Three-dimensional open nano-netcage electrocatalysts for efficient pH-universal overall water splitting. *Nat. Commun.* **10**, 4875 (2019).

4 Morales-Guio, C. G., Stern, L.-A. & Hu, X. Nanostructured hydrotreating catalysts for electrochemical hydrogen evolution. *Chem. Soc. Rev.* **43**, 6555-6569 (2014).

5 Zou, X. & Zhang, Y. Noble metal-free hydrogen evolution catalysts for water splitting. *Chem. Soc. Rev.* **44**, 5148-5180 (2015).

6 Zhang, B. *et al.* Homogeneously dispersed multimetal oxygen-evolving catalysts. *Science* **352**, 333-337 (2016).

7 Zhang, Q., Bedford, N. M., Pan, J., Lu, X. & Amal, R. A fully reversible water electrolyzer cell made up from FeCoNi (Oxy)hydroxide atomic layers. *Advanced Energy Materials* **9**, 1901312 (2019).

8 Cui, Y. *et al.* Trace oxophilic metal induced surface reconstruction at buried RuRh cluster interfaces possesses extremely fast hydrogen redox kinetics. *Nano Energy* **90**, 106579 (2021).

9 Kim, H. *et al.* Identification of single-atom Ni site active toward electrochemical CO_2 conversion to CO. *J. Am. Chem. Soc.* **143**, 925-933 (2021).

10 Liang, J. *et al.* Bowl-like SnO_2@carbon hollow particles as an advanced anode material for Lithium-Ion batteries. *Angew. Chem. Int. Edit.* **53**, 12803-12807 (2014).

11 Görlin, M. *et al.* Oxygen evolution reaction dynamics, faradaic charge efficiency, and the active metal redox states of Ni–Fe oxide water splitting electrocatalysts. *Journal of the American Chemical Society* **138**, 5603-5614 (2016).

12 Zhai, P. *et al.* Engineering single-atomic ruthenium catalytic sites on defective nickel-iron layered double hydroxide for overall water splitting. *Nat. Commun.* **12**, 4587 (2021).

13 Zhou, L., Zhang, C., Zhang, Y., Li, Z. & Shao, M. Host modification of layered double hydroxide electrocatalyst to boost the thermodynamic and kinetic activity of oxygen evolution reaction. *Adv. Funct. Mater.* **31**, 2009743 (2021).

14 Kang, J. *et al.* Valence oscillation and dynamic active sites in monolayer NiCo hydroxides for water oxidation. *Nat. Catal.* **4**, 1050-1058 (2021).

15 Chala, S. A. *et al.* Site activity and population engineering of NiRu-layered double hydroxide nanosheets decorated with silver nanoparticles for oxygen evolution and reduction reactions. *ACS Catal.* **9**, 117-129 (2019).

16 Zhang, S. L. *et al.* Metal atom-doped Co_3O_4 hierarchical nanoplates for electrocatalytic oxygen evolution. *Adv. Mater.* **32**, 2002235 (2020).

17 Lu, X. & Zhao, C. Electrodeposition of hierarchically structured three-dimensional nickel–iron electrodes for efficient oxygen evolution at high current densities. *Nat. Commun.* **6**, 6616 (2015).

18 Chen, Z. *et al.* Oriented transformation of Co-LDH into 2D/3D ZIF-67 to achieve Co–N–C hybrids for efficient overall water splitting. *Adv. Energy Mater.* **9**, 1803918 (2019).

19 He, D. *et al.* Active electron density modulation of Co_3O_4-based catalysts enhances their oxygen evolution performance. *Angew. Chem. Int. Edit.* **59**, 6929-6935 (2020).

20 Wu, Z.-P. *et al.* Manipulating the local coordination and electronic structures for efficient electrocatalytic oxygen evolution. *Adv. Mater.* **33**, 2103004 (2021).

21 Jiao, L. *et al.* Non-bonding interaction of neighboring Fe and Ni single-atom pairs on MOF-derived N-doped carbon for enhanced CO_2 electroreduction. *J. Am. Chem. Soc.* **143**, 19417-19424 (2021).

22 Chen, K. *et al.* Ultrasonic plasma engineering toward facile synthesis of single-atom M-N_4/N-doped carbon (M = Fe, Co) as superior oxygen electrocatalyst in rechargeable zinc–air batteries. *Nano-Micro*

Lett. **13**, 60 (2021).

23 Hu, X. *et al.* Ru single atoms on N-doped carbon by spatial confinement and ionic substitution strategies for high-performance Li–O_2 batteries. *J. Am. Chem. Soc.* **142**, 16776-16786 (2020).

24 Kibsgaard, J., Jaramillo, T. F. & Besenbacher, F. Building an appropriate active-site motif into a hydrogen-evolution catalyst with thiomolybdate $[Mo_3S_{13}]_2$–clusters. *Nat. Chem.* **6**, 248-253 (2014).

25 Li, F. *et al.* Balancing hydrogen adsorption/desorption by orbital modulation for efficient hydrogen evolution catalysis. *Nat. Commun.* **10**, 4060 (2019).

26 Chen, D. *et al.* Ultralow Ru loading transition metal phosphides as high-efficient bifunctional electrocatalyst for a solar-to-hydrogen generation system. *Adv. Energy Mater.* **10**, 2000814 (2020).

27 Wen, C. *et al.* Roles of the narrow electronic band near the Fermi level in 1T-TaS_2 related layered materials. *Phys. Rev. Lett.* **126**, 256402 (2021).

28 Pham, P. V. *et al.* 2D Heterostructures for ubiquitous electronics and optoelectronics: principles, opportunities, and challenges. *Chem. Rev.* DOI:10.1021/acs.chemrev.1c00735 (2022).

29 Lei, L. *et al.* Demystifying the active roles of NiFe-based oxides/(oxy)hydroxides for electrochemical water splitting under alkaline conditions. *Coordin. Chem. Rev.* **408**, 213177 (2020).

30 Guo, Y. *et al.* Low-temperature CO_2 methanation over CeO_2-supported Ru single atoms, nanoclusters, and nanoparticles competitively tuned by strong metal–support interactions and H-spillover effect. *ACS Catal.* **8**, 6203-6215 (2018).

31 Su, P. *et al.* Exceptional electrochemical her performance with enhanced electron transfer between ru nanoparticles and single atoms dispersed on a carbon substrate. *Angew. Chem. Int. Edit.* **60**, 16044-16050 (2021).

32 Bai, J. *et al.* Molybdenum-promoted surface reconstruction in polymorphic cobalt for initiating rapid oxygen evolution. *Adv. Energy Mater.* **12**, 2103247 (2022).

Declarations

Acknowledgements

This work was supported by the National Natural Science Foundation of China (NSFC) (21501096, 22075223), and Natural Science Foundation of Jiangsu (BK20150086, BK20201120), Foundation of the Jiangsu Education Committee (15KJB150020), the Six Talent Peaks Project in Jiangsu Province (JY-087), and Innovation Project of Jiangsu Province.

Author contributions

S.L.L. and S.C.M. conceived the project and oversaw all the research phases. S.L.L. and X.Q.M. designed the experiment. S.L.L. and X.Q.M. carried out the theoretical studies. S.P.D. and J.B.C. synthesized and characterized the samples. X.Q.M. and X.Y.G. carried out the electrochemical experiments and data analysis. X.Q.M., X.Y.G., S.P.D., Q.C. and W.X.C. were involved in the TEM, XRD, XPS, and XAFS characterizations and data analysis. X.Q.M., X.Y.G., S.P.D., M.Y. and C.Y.C. discussed the results. S.L.L. and X.Q.M. wrote the paper. All the authors contributed to and commented on this paper.

Figures

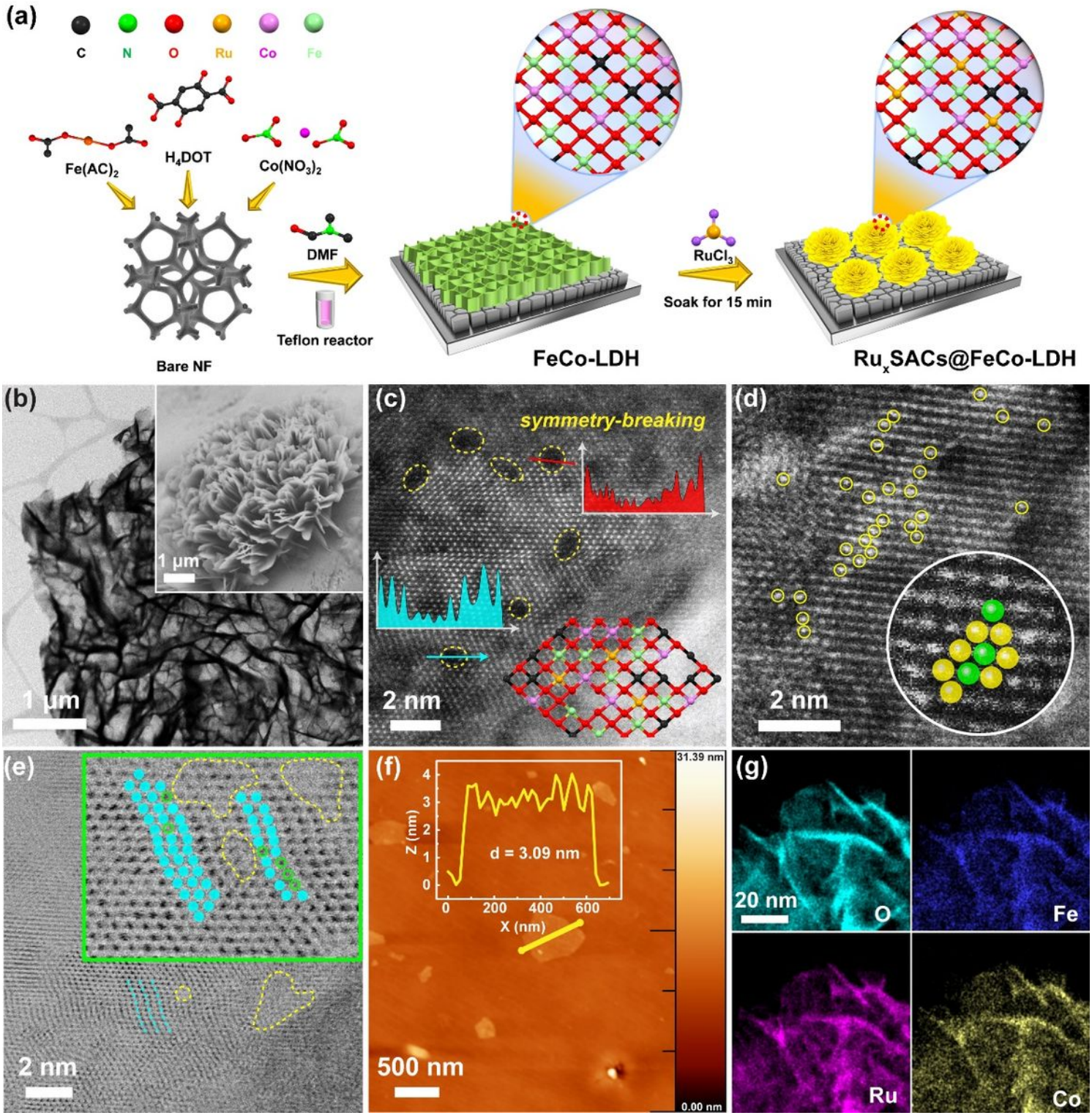

Figure 1

(a) Synthesis illustration, (b) TEM and FE-SEM images, (c-d) HAADF-STEM image and (e) HRTEM images, (f) AFM image and the corresponding AFM height profiles, (g) elemental mapping images of Ru_1 SACs@FeCo-LDH.

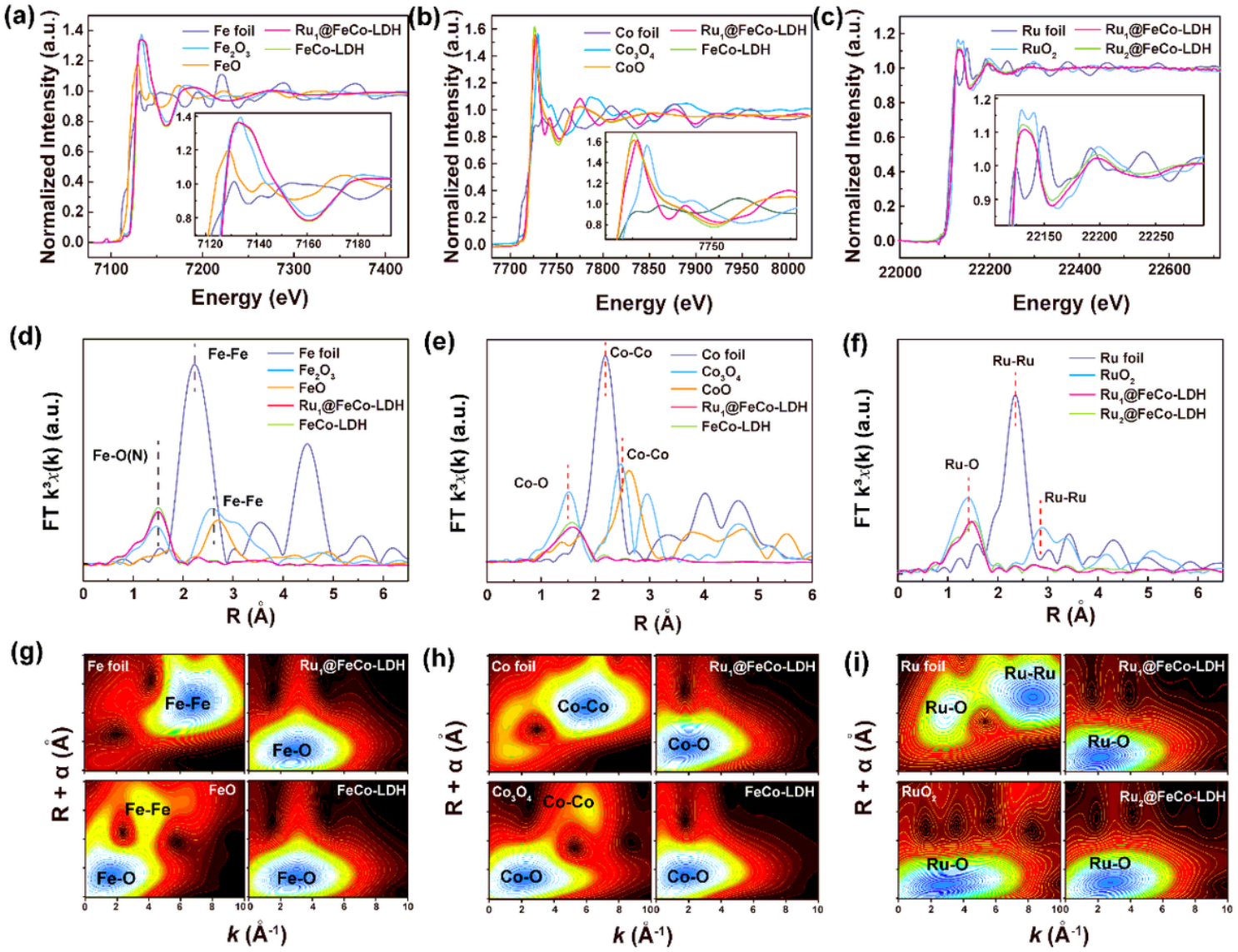

Figure 2

(a) Fe K-edge, (b) Co K-edge and (c) Ru K-edge XANES spectra of Ru SACs@FeCo-LDH obtained using Co foil and standard CoO or Co_3O_4 powders as references, respectively. Wavelet transforms for the k^3-weighted EXAFS signals of the (d) Fe K-edge and (e) Co K-edge for Ru_1 SACs@FeCo-LDH, FeCo-LDH, Co foil and standard CoO or Co_3O_4 powders, respectively; (f) Ru K-edge for Ru_x SACs@FeCo-LDH, Ru foil and standard RuO_2 powders, respectively; (g-i) Fourier transformed (FT) k^3-weighted χ(k)-function of the EXAFS spectra for the Co K-edge, Fe K-edge, and Ru K-edge, respectively.

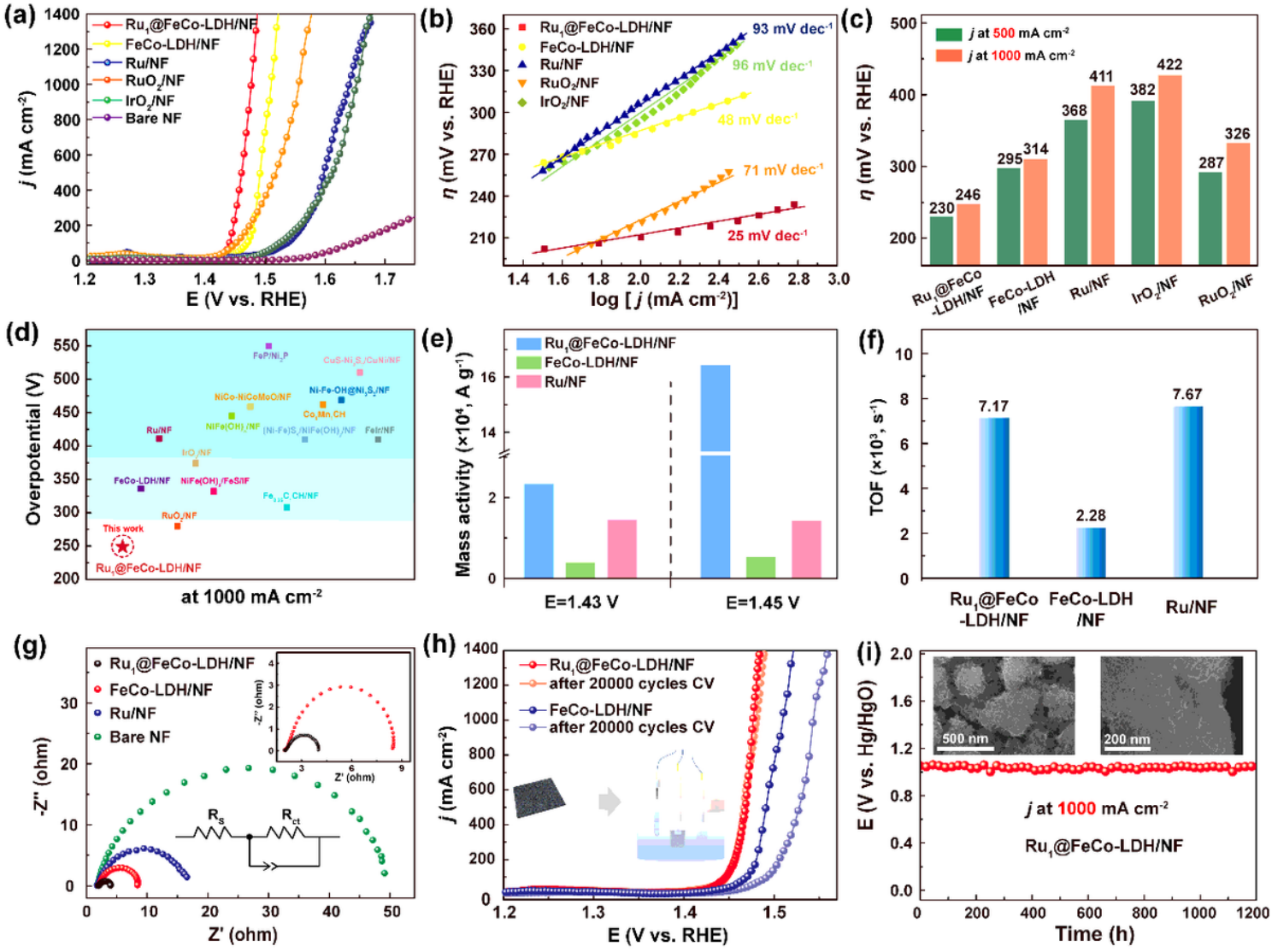

Figure 3

(a) Polarization curves in 1.0 M KOH; (b) The corresponding Tafel plots; (c) Comparison of overpotential at 500 mA cm^{-2} and 1 A cm^{-2} for OER electrocatalysis, respectively; (e) In 1.0 M KOH solution, compared with the recently reported OER catalyst overpotential at 1 A cm^{-2}; (e) Comparison of MA at different overpotential; (f) Potential-dependent TOF curves and exchange current density (j_0); (g) Nyquist plots. (h) Polarization curves for Ru_1 SACs@FeCo-LDH and FeCo-LDH before and after 20000 cycles CV; (i) Chronopotentiometry curve of Ru_1 SACs@FeCo-LDH under the temporal evolution of the potential required to maintain 1 A cm^{-2} for 1000 h.

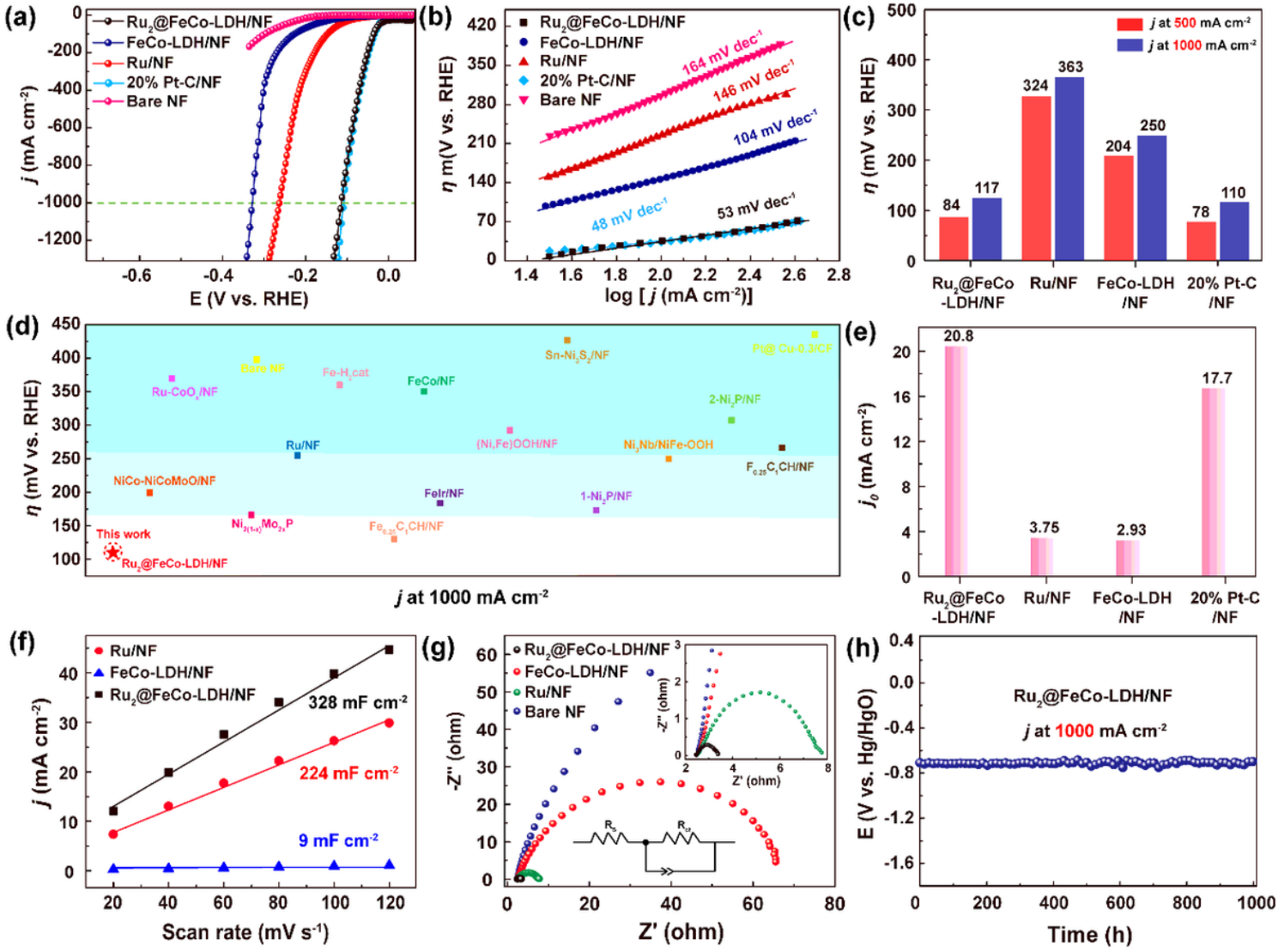

Figure 4

(a) Polarization curves in 1 M KOH; (b) The corresponding Tafel plots; (c) Comparison of overpotential at 500 mA cm^{-2} and 1 A cm^{-2} for OER electrocatalysis, respectively; (d) In 1.0 M KOH solution, compared with the recently reported OER catalyst overpotential at 1 A cm^{-2}; (e) Comparison of exchange current density (j_0), (f) Calculated C_{dl} and (g) Nyquist plots. (h) Chronopotentiometry curve of Ru_2 SACs@FeCo-LDH under the temporal evolution of the potential required to maintain 1 A cm^{-2} for 1000 h.

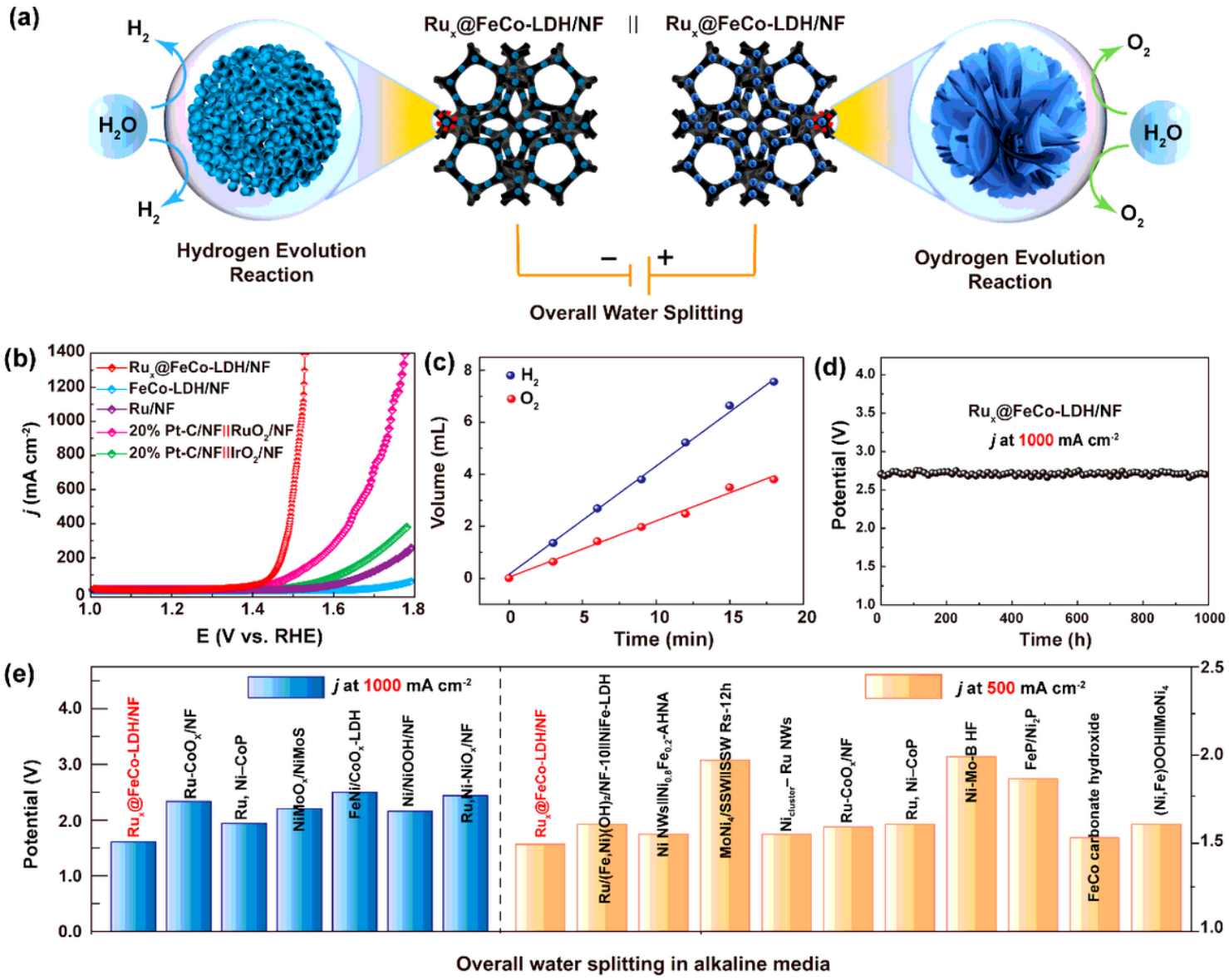

Figure 5

(a) Schematic representation of overall water splitting process; (b) polarization curves of the bifunctional Ru_x SACs@FeCo-LDH electrocatalyst; (c) The amount of gas theoretically calculated and experimentally measured vs. time by use of Ru_1 SACs@FeCo-LDH; (d) Chronopotentiometry curve of Ru_1 SACs@FeCo-LDH under the overall water splitting of the potential required to maintain 1 A cm^{-2} for 1000 h; (e) comparison of the cell voltages at 1 A cm^{-2} for Ru_1 SACs@FeCo-LDH with reported bifunctional electrocatalysts.

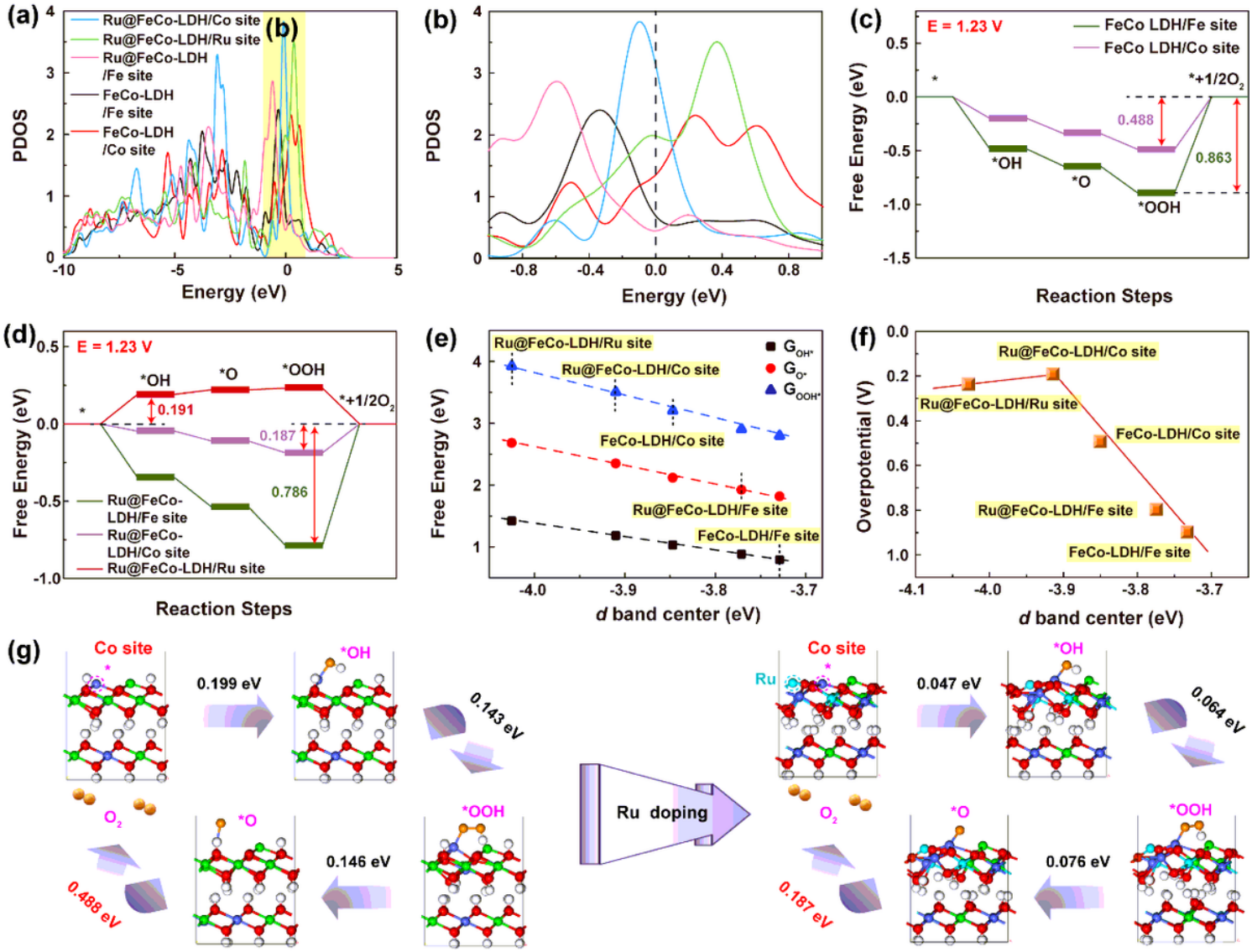

Figure 6

(a), (b) Calculated density of states for Fe, Co and Ru active sites over the Ru SACs@FeCo-LDH and FeCo-LDH. (c) Energy profile for the OER process on the FeCo-LDH and (d) Ru SACs@FeCo-LDH. (e) Scaling relation between ΔG_{OOH*}, ΔG_{OH*}, ΔG_{O*} and *d*-band centers. (f) Volcano plot of overpotential as a function of *d*-band centers. (g) Representative OER mechanism over the FeCo-LDH and Ru SACs@FeCo-LDH.

Supplementary Files

This is a list of supplementary files associated with this preprint. Click to download.

- SI.docx